Total internal reflection: a deeper look

A. I. Mahan and C. V. Bitterli

In the present paper, we have presented a Maxwellian boundary-type solution for total internal reflection with unbounded incident waves at an interface between two nonabsorbing media, in which the instantaneous, time varying, and time averaged radiant fluxes have been determined at all points in the two media. Solutions for the *s* and *p* polarizations were found for which the instantaneous tangential **E** and **H** components and normal components of the radiant flux were continuous in crossing the interface. From these radiant fluxes, it was possible to derive equations for the flow lines, to determine the instantaneous radiant fluxes along these flow lines, and to see how the methods of propagation differed in the two media and for the two polarizations. At the interface, the flow lines and their radiant fluxes experience unusual reflection and refraction processes, follow curved flow lines in the second medium, and return into the first medium with boundary conditions, which are mirror images of those at the points of incidence. These unfamiliar processes in the second medium are due to inhomogeneous waves, whose properties have not been understood. When these instantaneous solutions are extended to time varying and time averaged radiant fluxes, it is interesting to see how incident planes of constant radiant flux and phase experience such complex processes in the second medium and are still able to generate other reflected planes of constant radiant flux and phase in the first medium. These ideas prescribe specific detailed functions for the **E** and **H** fields and radiant fluxes in the second medium, which help to answer many long standing questions about the physical processes involved in total internal reflection.

Introduction

Total internal reflection in nonabsorbing media has been of continuing interest over the years.[1] The primary reasons for this have been that present theories for unbounded incident waves predict that, in the time average, all the radiant flux incident beyond the critical angle on an interface between two nonabsorbing media is reflected, no radiant flux flows across the interface in the direction of the surface normals, and a radiant flux flow appears in the second medium in a direction parallel to the interface.[2] There is then apparently a paradox, for one can ask how it is possible to have a radiant flux flow in the second medium and simultaneously have total internal reflection in the first medium? A closely related question, of course, is what are the sources and functions of these radiant fluxes in the second medium? To answer these questions, it is necessary to look in detail at the magnitudes and phases of the radiant fluxes and the geometries of their associated radiant flux flow lines in both media under steady state, time changing, and time average conditions. Unfortunately, instantaneous and time changing solutions have been largely neglected,[2] for it is much simpler to use complex **E** and **H** fields and the complex Poynting vector,[3] to calculate the more useful time averages of the reflected radiant fluxes, and not to consider what happens in the second medium. It is becoming more difficult, however, to avoid these problems, for, in addition to appearing in the optical region,[4] these so-called "up and over waves" are reappearing in long wavelength regions and creating easily observable unfamiliar problems.[5] There is then a need for a deeper detailed theoretical study, if total internal reflection is to be understood.

In the present paper, the authors would like to present their ideas on a more complete solution for total internal reflection, in which the properties of unbounded instantaneous radiant fluxes and their associated flow lines have been followed through both media under steady state, time changing, and time average conditions. For this solution, homogeneous, transverse plane polarized waves are incident on the interface beyond the critical angle, and both reflected and transmitted waves of different amplitudes and phases appear along the interface. The usual boundary conditions involving the continuity of the tangential **E** and **H** fields are used to determine the amplitudes and phases of these reflected and transmitted waves, and all the components are written in their real instantaneous forms. It is also possible from these **E** and **H** fields to write down the corresponding real instantaneous com-

The authors are with Johns Hopkins University, Applied Physics Laboratory, Laurel, Maryland 20810.

Received 25 April 1977.
0003-6935/78/0215-0509$0.50/0.

ponents of the Poynting vector, from which the slopes of the flow lines and the equations for the flow lines can be obtained. From these equations, one can then make simultaneous studies of these radiant fluxes and their associated flow lines in both media under steady state, time changing, and time average conditions and learn in detail just how these radiant fluxes flow into and out of the second medium. In our paper, we have placed primary emphasis on trying to understand the physics of these processes and have provided several figures showing the calculated forms of the radiant fluxes and flow lines under steady state, time changing, and time average conditions. These studies provide an informative and realistic description of the physical processes associated with total internal reflection.

Electric Vector Perpendicular to Plane of Incidence

The starting point for such a paper must be Maxwell's equations. For nonabsorbing and nonmagnetic media, these equations are limited to

$$Curl\ \mathbf{E} = -\frac{1}{c}\frac{\partial \mathbf{H}}{\partial t},\quad Curl\ \mathbf{H} = \frac{\epsilon}{c}\frac{\partial \mathbf{E}}{\partial t},\qquad \text{div}\mathbf{D} = \text{div}\mathbf{H} = 0, \tag{1}$$

where ϵ is a real dielectric constant characteristic of the medium under consideration. If we polarize the incident plane wave so that the electric vector in Fig. 1 lies along the y axis ($E_x = E_z = 0$), Eqs. (1) reduce to the following more useful equations:

$$\frac{\partial E_y}{\partial z} = \frac{1}{c}\frac{\partial H_x}{\partial t},\quad \frac{\partial E_y}{\partial x} = -\frac{1}{c}\frac{\partial H_z}{\partial t},\quad \frac{\partial H_x}{\partial z} - \frac{\partial H_z}{\partial x} = \frac{\epsilon}{c}\frac{\partial E_y}{\partial t}. \tag{2}$$

These equations can be solved simultaneously for E_y, and we find that E_y must satisfy

$$\frac{\partial^2 E_y}{\partial x^2} + \frac{\partial^2 E_y}{\partial z^2} = \frac{\epsilon}{c^2}\frac{\partial^2 E_y}{\partial t^2}, \tag{3}$$

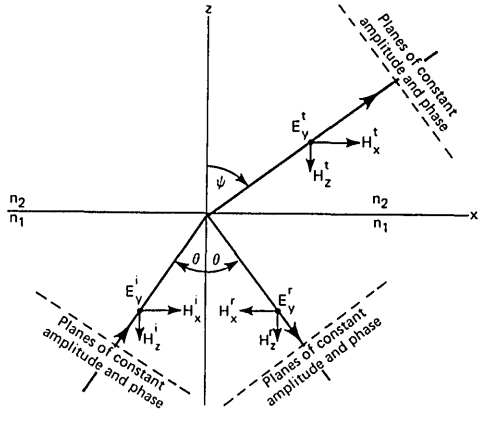

Fig. 1. Reflection and refraction for s polarization at interface between two absorbing media with angles of incidence below critical angle.

which is the familiar wave equation. The solutions to this equation and Eqs. (2) fix the general forms of the electromagnetic waves in both media. The **E** and **H** components for these incident, reflected, and transmitted waves, in the region below the critical angle, except for certain boundary considerations,[6] are

$$\begin{aligned}
E_y^i &= E_s \exp\left\{i\left[\omega t - \frac{\omega}{c}n_1(x\sin\varphi + z\cos\varphi)\right]\right\},\\
H_x^i &= -n_1\cos\varphi E_s \exp\left\{i\left[\omega t - \frac{\omega}{c}n_1(x\sin\varphi + z\cos\varphi)\right]\right\},\\
H_z^i &= n_1\sin\varphi E_s \exp\left\{i\left[\omega t - \frac{\omega}{c}n_1(x\sin\varphi + z\cos\varphi)\right]\right\},\\
E_y^r &= R_s \exp\left\{i\left[\omega t - \frac{\omega}{c}n_1(x\sin\varphi - z\cos\varphi)\right]\right\},\\
H_x^r &= n_1\cos\varphi R_s \exp\left\{i\left[\omega t - \frac{\omega}{c}n_1(x\sin\varphi - z\cos\varphi)\right]\right\},\\
H_z^r &= n_1\sin\varphi R_s \exp\left\{i\left[\omega t - \frac{\omega}{c}n_1(x\sin\varphi - z\cos\varphi)\right]\right\},\\
E_y^t &= D_s \exp\left\{i\left[\omega t - \frac{\omega}{c}n_2(x\sin\psi + z\cos\psi)\right]\right\},\\
H_x^t &= -n_2\cos\psi D_s \exp\left\{i\left[\omega t - \frac{\omega}{c}n_2(x\sin\psi + z\cos\psi)\right]\right\},\\
H_z^t &= n_2\sin\psi D_s \exp\left\{i\left[\omega t - \frac{\omega}{c}n_2(x\sin\psi + z\cos\psi)\right]\right\}.
\end{aligned} \tag{4}$$

In these equations, $n_1 = (\epsilon_1)^{1/2}$ and $n_2 = (\epsilon_2)^{1/2}$ are the refractive indices of both media, and these are plane, homogeneous transverse waves, whose planes of constant amplitude and phase are indicated in Fig. 1 and will be of interest in this paper. These waves must also satisfy the before mentioned boundary conditions[6] and, to be useful for our problem, limited to angles of incidence beyond the critical angle. If, then, we make the tangential components E_y and H_x in Fig. 1 continuous in crossing the boundary, we find that

$$n_1\sin\varphi = n_2\sin\psi, \tag{5}$$

which is Snell's law and is useful in regions below the critical angle. In regions beyond the critical angle,[7] however,

$$\sin\psi = \frac{n_1}{n_2}\sin\varphi > 1,\qquad \cos\psi = -i\left(\frac{n_1^2}{n_2^2}\sin^2\psi - 1\right)^{1/2} \tag{6}$$

When we substitute Eq. (5) and Eq. (6) in these continuity equations, R_s and D_s will be found to have the values

$$R_s = E_s\exp(i\delta_s{}^r),\qquad D_s = \frac{2n_1\cos\varphi}{(n_1{}^2 - n_2{}^2)^{1/2}}E_s\exp(i\delta_s{}^t), \tag{7}$$

where the indicated phase changes after reflection and transmission are given by

$$\tan\frac{\delta_s{}^r}{2} = \tan\delta_s{}^t = \frac{(n_1{}^2\sin^2\varphi - n_2{}^2)^{1/2}}{n_1\cos\varphi}. \tag{8}$$

Equations (6), (7), and (8) can now be substituted in Eqs. (4) to obtain the real instantaneous **E** and **H** components in the region beyond the critical angle, which are

$$E_y{}^i = E_s \cos\left[\omega t - \frac{2\pi}{\lambda_1}(x\sin\varphi + z\cos\varphi)\right],$$

$$H_x{}^i = -n_1\cos\varphi E_s \cos\left[\omega t - \frac{2\pi}{\lambda_1}(x\sin\varphi + z\cos\varphi)\right],$$

$$H_z{}^i = n_1\sin\varphi E_s \cos\left[\omega t - \frac{2\pi}{\lambda_1}(x\sin\varphi + z\cos\varphi)\right],$$

$$E_y{}^r = E_s \cos\left[\omega t - \frac{2\pi}{\lambda_1}(x\sin\varphi - z\cos\varphi) + \delta_s{}^r\right],$$

$$H_x{}^r = n_1\cos\varphi E_s \cos\left[\omega t - \frac{2\pi}{\lambda_1}(x\sin\varphi - z\cos\varphi) + \delta_s{}^r\right],$$

$$H_z{}^r = n_1\sin\varphi E_s \cos\left[\omega t - \frac{2\pi}{\lambda_1}(x\sin\varphi - z\cos\varphi) + \delta_s{}^r\right],$$

$$E_y{}^t = \frac{2n_1\cos\varphi}{(n_1{}^2 - n_2{}^2)^{1/2}} E_s \exp\left[-\frac{2\pi}{\lambda_1} z\left(\sin^2\varphi - \frac{n_2{}^2}{n_1{}^2}\right)^{1/2}\right] \times \cos\left(\omega t - \frac{2\pi}{\lambda_1} x\sin\varphi + \delta_s{}^t\right),$$

$$H_x{}^t = -\frac{2n_1\cos\varphi(n_1{}^2\sin^2\varphi - n_2{}^2)^{1/2}}{(n_1{}^2 - n_2{}^2)^{1/2}} E_s \times \exp\left[-\frac{2\pi}{\lambda_1} z\left(\sin^2\varphi - \frac{n_2{}^2}{n_1{}^2}\right)^{1/2}\right] \sin\left(\omega t - \frac{2\pi}{\lambda_1} x\sin\varphi + \delta_s{}^t\right),$$

$$H_z{}^t = \frac{2n_1{}^2\sin\varphi\cos\varphi}{(n_1{}^2 - n_2{}^2)^{1/2}} E_s \exp\left[-\frac{2\pi}{\lambda_1} z\left(\sin^2\varphi - \frac{n_2{}^2}{n_1{}^2}\right)^{1/2}\right] \cos\left(\omega t - \frac{2\pi}{\lambda_1} x\sin\varphi + \delta_s{}^t\right). \quad (9)$$

The waves in the second medium are inhomogeneous plane waves traveling along the x direction with planes of constant phase normal to x and planes of constant amplitude normal to z. Like all inhomogeneous waves,[8] they also have a longitudinal component, which, for this plane of polarization, is $H_x{}^t$.

Since we know the forms of the **E** and **H** components in both media, it is possible to write down the real instantaneous components of the Poynting vector, which describe the radiant flux densities. Clearly, there are only going to be P_x and P_z components, and these are

$$P_x{}^i(s) = \frac{c}{4\pi} n_1\sin\varphi E_s{}^2 \cos^2\left[\omega t - \frac{2\pi}{\lambda_1}(x\sin\varphi + z\cos\varphi)\right],$$

$$P_z{}^i(s) = \frac{c}{4\pi} n_1\cos\varphi E_s{}^2 \cos^2\left[\omega t - \frac{2\pi}{\lambda_1}(x\sin\varphi + z\cos\varphi)\right],$$

$$P_x{}^r(s) = \frac{c}{4\pi} n_1\sin\varphi E_s{}^2 \cos^2\left[\omega t - \frac{2\pi}{\lambda_1}(x\sin\varphi - z\cos\varphi) + \delta_s{}^r\right],$$

$$P_z{}^r(s) = -\frac{c}{4\pi} n_1\cos\varphi E_s{}^2 \cos^2\left[\omega t - \frac{2\pi}{\lambda_1}(x\sin\varphi - z\cos\varphi) + \delta_s{}^r\right],$$

$$P_x{}^t(s) = \frac{c}{4\pi}\frac{4n_1{}^3\sin\varphi\cos^2\varphi}{n_1{}^2 - n_2{}^2} E_s{}^2 \times \exp\left[-\frac{4\pi}{\lambda_1} z\left(\sin^2\varphi - \frac{n_2{}^2}{n_1{}^2}\right)^{1/2}\right] \cos^2\left(\omega t - \frac{2\pi x}{\lambda_1}\sin\varphi + \delta_s{}^t\right),$$

$$P_z{}^t(s) = \frac{c}{4\pi}\frac{4n_1{}^2\cos^2\varphi(n_1{}^2\sin^2\varphi - n_2{}^2)^{1/2}}{n_1{}^2 - n_2{}^2} E_s{}^2 \times \exp\left[-\frac{4\pi}{\lambda_1} z\left(\sin^2\varphi - \frac{n_2{}^2}{n_1{}^2}\right)^{1/2}\right] \times \cos\left(\omega t - \frac{2\pi x}{\lambda_1}\sin\varphi + \delta_s{}^t\right)\sin\left(\omega t - \frac{2\pi x}{\lambda_1}\sin\varphi + \delta_s{}^t\right). \quad (10)$$

Since we know the components of the Poynting vector in each medium, it should be clear, following Eichenwald,[9] that the slopes of the corresponding radiant flux flow lines in both media are

$$\left(\frac{dz}{dx}\right)_i = \frac{P_z{}^i(s)}{P_x{}^i(s)} = \cot\varphi, \quad \left(\frac{dz}{dx}\right)_r = \frac{P_z{}^r(s)}{P_x{}^r(s)} = -\cot\varphi,$$

$$\left(\frac{dz}{dx}\right)_t = \frac{P_z{}^t(s)}{P_x{}^t(s)} = \frac{(n_1{}^2\sin^2\varphi - n_2{}^2)^{1/2}}{n_1\sin\varphi} \times \tan\left(\omega t - \frac{2\pi x}{\lambda_1}\sin\varphi + \delta_s{}^t\right). \quad (11)$$

These equations can be integrated so that the radiant flux flow lines in both media are described by

$$z^i(s) = (x - x_{1s}{}^i)\cot\varphi, \; z^r(s) = -(x - x_{1s}{}^r)\cot\varphi,$$

$$z^t(s) = \frac{\lambda_1(n_1{}^2\sin^2\varphi - n_2{}^2)^{1/2}}{2\pi n_1\sin^2\varphi}\left\{\log_e\left[\cos\left(\omega t - \frac{2\pi}{\lambda_1} x\sin\varphi + \delta_s{}^t\right)\right] - \log_e\left[\cos\left(\omega t - \frac{2\pi}{\lambda_1} x_{1s}{}^t\sin\varphi + \delta_s{}^t\right)\right]\right\}, \quad (12)$$

in which the $x_{1s}{}^i$, $x_{1s}{}^r$, and $x_{1s}{}^t$ are the x values for which $z^i(s) = z^r(s) = z^t(s) = 0$. The flow lines in the first medium are straight lines, but those in the second medium are curved, are all the same shape, as described by the first term, but have different depths of penetration, as described by the second term. These radiant fluxes and flow lines in Eqs. (10) and (12) will be of primary interest in this paper.

To understand the propagation characteristics of these radiant fluxes, we have in Fig. 2 plotted calculated instantaneous $P_x{}^i(s)$, $P_z{}^i(s)$, $P_x{}^r(s)$, $P_z{}^r(s)$, $P_x{}^t(s)$, and $P_z{}^t(s)$ values for $n_1 = 1.5$, $n_2 = 1.0$, $\varphi = 45°$, and $z = t = 0$ to see what is happening along the interface. Fortunately, $P_x{}^i(s)$ *and* $P_z{}^i(s)$ are of the same form, are always positive, and have the same period $\lambda_1/2\sin\varphi$ along the x axis. $P_x{}^r(s)$ and $P_z{}^r(s)$ are also of the same form, but $P_z{}^r(s)$ is of opposite sign, and both $P_x{}^r(s)$ and $P_z{}^r(s)$

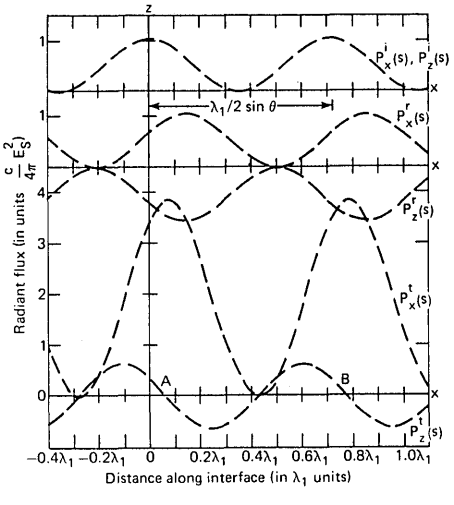

Fig. 2. Components of incident, reflected, and transmitted radiant fluxes for s polarization along interface (in units of λ_1) for $n_1 = 1.5$, $n_2 = 1.0$, $\varphi = 45°$, and $z = t = 0$.

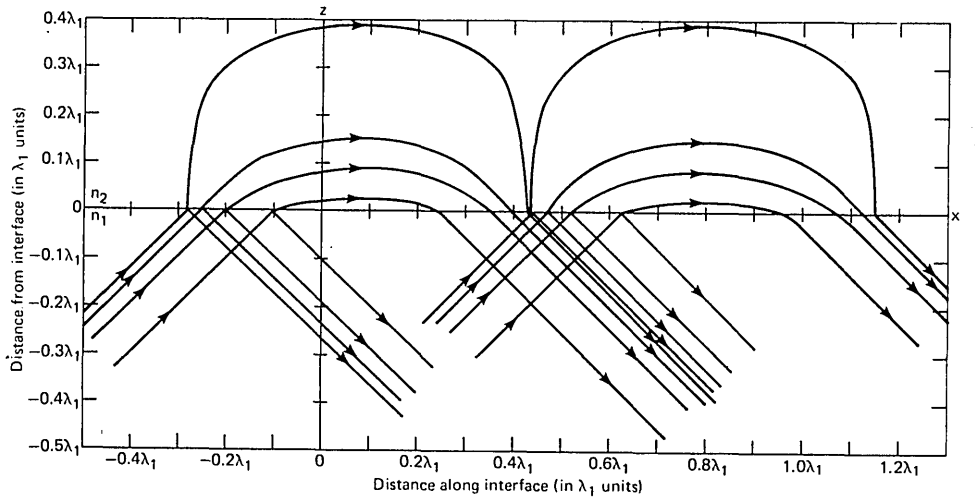

Fig. 3. Radiant flux flow lines $z^i(s)$, $z^r(s)$, and $z^t(s)$ for s polarization with $n_1 = 1.5$, $n_2 = 1.0$, $\varphi = 45°$, and $t = 0$ when $x_{1s}{}^i = x_{1s}{}^r = x_{1s}{}^t = -0.1\lambda_1, -0.2087\lambda_1, -0.25\lambda_1$, and $-0.28\lambda_1$.

are shifted to the right by $[\lambda_1/(2\pi \sin\varphi)]\delta_s{}^r$, corresponding to the advance in phase $\delta_s{}^r$ after reflection. $P_x{}^t(s)$ is also similar in form, but is of much larger magnitude and is shifted to the right by $[\lambda_1/(2\pi \sin\varphi)]\delta_s{}^t$, corresponding to the advance in phase $\delta_s{}^t$ experienced on crossing the interface. $P_z{}^t(s)$, however, is more interesting, for it too is shifted to the right by this same amount, but is alternately positive and negative, suggesting varying inflows and outflows of radiant flux along the interface in the second medium with the same period $\lambda_1/2 \sin\varphi$. These curves, to be sure, show that the $P_z(s)$ components are continuous across the interface for all values of x, but at points to the left of the zeroes at A and B in the $P_z{}^t(s)$ curve, corresponding to inflows of radiant flux into the second medium, these boundary conditions indicate that

$$|P_z{}^i(s)|_{\text{in}} = |P_z{}^r(s)|_{\text{in}} + |P_z{}^t(s)|_{\text{in}}, \tag{13}$$

while to the right of these same points in regions of outflows of radiant flux,

$$|P_z{}^r(s)|_{\text{out}} = |P_z{}^i(s)|_{\text{out}} + |P_z{}^t(s)|_{\text{out}}. \tag{14}$$

At this point in the discussion, one can only ask how it is possible for $|P_z{}^r(s)|_{\text{out}}$ to be larger than $|P_z{}^i(s)|_{\text{out}}$, and the $|P_x{}^t(s)|_{\text{in}}$ and $|P_x{}^t(s)|_{\text{out}}$ have much larger values than $|P_x{}^i(s)|_{\text{in}}$ and $|P_x{}^i(s)|_{\text{out}}$, which are difficult to understand.

Our next step is to look at the instantaneous flow lines in both media, whose forms are determined by Eqs. (12). In Fig. 3, we have plotted some calculated flow lines for the same range of x values in Fig. 2 and for the same n_1, n_2, φ, and t values. The chosen x_{1s} values were $-0.1\lambda_1$, $-0.2087\lambda_1$, $-0.25\lambda_1$, and $-0.28\lambda_1$. Within each cyclic group of period $\lambda_1/2 \sin\varphi$, there are infinite numbers of flow lines, whose shapes in the second medium are the same, but have different depths of penetration. The flow line at $-0.28\lambda_1$ is very close to the outside limiting flow line at

$$-\frac{2\pi}{\lambda_1} x_{1s} \sin\varphi + \delta_s{}^t = \frac{\pi}{2} \tag{15}$$

and has $z^t(s)$ values of the same form extending to and returning from infinity. The flow line originating at $x_{1s} = -0.2087\lambda_1$ is particularly interesting, for it crosses over into the second medium and returns to the first without refraction. Other flow lines at x_{1s} values to the left of this flow line are refracted in counterclockwise directions at the points of incidence and reentrance into the first medium, but flow lines to the right are refracted in clockwise directions. These are unfamiliar refraction properties, but the magnitudes and signs of the refraction angles can be readily checked from Eqs. (11) and Fig. 2.

The flow lines in Fig. 3, thus far, have added very little to our understanding of total internal reflection other than calling attention to their existence and geometry. Now, however, we are in a position to learn much more about total internal reflection by utilizing both the radiant fluxes and flow lines simultaneously. For the radiant flux densities, however, we will use the magnitudes of the vectors in Eqs. (10), for these are the quantities usually associated with the measured radiant fluxes.[10] These are

$$|\mathbf{P}^i(s)| = \frac{c}{4\pi} n_1 E_s{}^2 \cos^2\left[\omega t - \frac{2\pi}{\lambda_1}(x \sin\varphi + z \cos\varphi)\right],$$

$$|\mathbf{P}^r(s)| = \frac{c}{4\pi} n_1 E_s{}^2 \cos^2\left[\omega t - \frac{2\pi}{\lambda_1}(x \sin\varphi - z \cos\varphi) + \delta_s{}^r\right],$$

$$|\mathbf{P}^t(s)| = \frac{c}{4\pi} \frac{4n_1{}^2 \cos^2\varphi}{n_1{}^2 - n_2{}^2} E_s{}^2 \exp\left[-\frac{4\pi z}{\lambda_1}\left(\sin^2\varphi - \frac{n_2{}^2}{n_1{}^2}\right)^{1/2}\right] \cdot \cos\left(\omega t - \frac{2\pi x}{\lambda_1}\sin\varphi + \delta_s{}^t\right) \cdot \left[n_1{}^2 \sin^2\varphi - n_2{}^2 \sin^2\left(\omega t - \frac{2\pi x}{\lambda_1}\sin\varphi + \delta_s{}^t\right)\right]^{1/2}. \tag{16}$$

In Fig. 4, we have considered only two flow lines, indicated by the dark full lines, originating at $x_{1s} = -0.1\lambda_1$, and $-0.2087\lambda_1$ in Fig. 3, and have plotted instantaneous $|\mathbf{P}^i(s)|$, $|\mathbf{P}^r(s)|$, and $|\mathbf{P}^t(s)|$ values from Eqs. (16) as dashed lines, in units of $[c/(4\pi)]E_s{}^2$, in directions normal to the flow line in question, using known (x,z) values

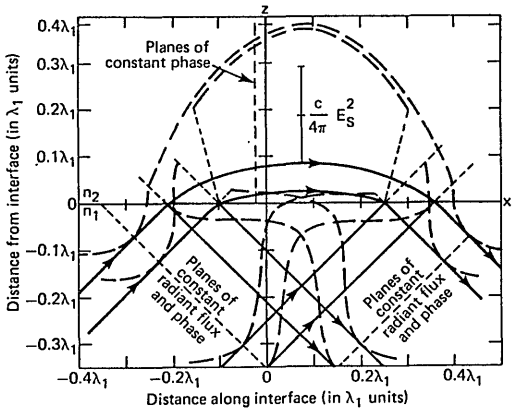

Fig. 4. Radiant flux and radiant flux flow lines for s polarization with $x_{1s} = -0.1\lambda_1$ and $-0.2087\lambda_1$, when $n_1 = 1.5$, $n_2 = 1.0$, $\varphi = 45°$, and $t = 0$.

from Eqs. (12). At each point of incidence on or emergence from the second medium, we have also plotted additional appropriate incident and reflected flow lines along which corresponding $|\mathbf{P}^i(s)|$ and $|\mathbf{P}^r(s)|$ values from Eqs. (16) are indicated. We can now, for the s polarization, give a clear physical picture of the phenomena involved in total internal reflection for this particular instantaneous case. In planes normal to the incident and reflected flow lines, one soon finds the expected planes of constant radiant flux and phase, which are common to all the flow lines in this cyclic group. The refracted flow lines, however, have no planes of constant radiant flux, but they do have planes of constant phase normal to the x direction, which are also common to all the flow lines in this cyclic group. For the outer flow line, whose x_{1s} is determined by

$$-\frac{2\pi}{\lambda_1} x_{1s} \sin\varphi + \delta_s{}^r = \frac{\pi}{2}, \tag{17}$$

the incident radiant flux passes through the interface in such a way that $|\mathbf{P}^i(s)|_{\text{in}} = |\mathbf{P}^t(s)|_{\text{in}}$ and $|\mathbf{P}^r(s)|_{\text{in}} = 0$. This particular flow line, then, passes through the interface without reflection losses and without refraction, and the normal components of the radiant flux are also continuous, as expected in Eq. (13). In the second medium, according to Eqs. (16), the refracted radiant fluxes experience exponential decreases determined by the distance from the interface. In Fig. 4, however, these losses, for such small z values, are more than compensated for by the decreasing cross sections due to the flow line shapes and continuous refraction from the point of incidence up to the peak position

$$-\frac{2\pi x}{\lambda_1} \sin\varphi + \delta_s{}^t = 0, \tag{18}$$

so that the peak $|\mathbf{P}^t(s)|$ in the second medium is much larger than the peak $|\mathbf{P}^i(s)|$ in the first medium. At the point of reentrance into the first medium

$$-\frac{2\pi x_{2s}}{\lambda_1} \sin\varphi = -\frac{\pi}{2}, \tag{19}$$

we now find that the changes in magnitude and phase are such that $|\mathbf{P}^r(s)|_{\text{out}} = |\mathbf{P}^t(s)|_{\text{out}}$ and $|\mathbf{P}^i(s)|_{\text{out}} = 0$, so that this flow line also passes through the interface without reflection losses and without refraction and has normal components which are continuous as predicted by Eq. (14). This flow line is then most interesting, for it enters and leaves the second medium without reflection losses and without refraction.

The radiant flux densities along the inner flow line in Fig. 4 have somewhat different properties. At the point of incidence, there is a clockwise refraction, and both reflected and transmitted radiant fluxes appear. There is also a discontinuity in the radiant flux, which is such that

$$|\mathbf{P}^i(s)|_{\text{in}} \cos\varphi = |\mathbf{P}^r(s)|_{\text{in}} \cos\varphi + |\mathbf{P}^t(s)|_{\text{in}} \cos\varphi', \tag{20}$$

where φ' (72.2205°) is the angle of refraction for the radiant flux determined by Eqs. (11). This, however, simply says again that the normal components of the radiant flux in Eq. (13) are continuous in crossing the interface. The planes of constant radiant flux and phase in the first medium and the planes of constant phase in the second medium are the same as those for the outer flow line, but the radiant fluxes in the second medium are somewhat larger because of the flow line shapes, refraction, and closer proximity to the interface. For the inner flow line, we see that the path in the second medium is shorter than that for the outer flow line and that the paths in the first medium, up to the point of incidence and after the point of reentrance, have been increased by equal amounts, so that the planes of constant phase in the second medium are the same for both flow lines. At the point of reentrance into the first medium, there is again a discontinuity in the radiant flux, but now we find that

$$|\mathbf{P}^r(s)|_{\text{out}} \cos\varphi = |\mathbf{P}^i(s)|_{\text{out}} \cos\varphi + |\mathbf{P}^t(s)| \cos\varphi', \tag{21}$$

so that the refraction is still in a clockwise direction, and the normal components of the radiant flux, as seen already in Eq. (14), are continuous in crossing the interface. In Fig. 5, we have also plotted similar calculations for the $x_{1s} = -0.28\lambda_1$ flow line, again using the $x_{1s} = -0.2087\lambda_1$ flow line as a reference. The primary differences here are that the refraction at the points of incidence on and reentrance from the second medium is now in a counterclockwise direction, the refracted radiant fluxes have much longer paths in the second medium, although still having the same planes of constant phase, and the exponential decreases in Eqs. (16) at these larger distances are beginning to reduce the radiant fluxes. If one continues these calculations with increasing negative x_{1s} values up to the limiting x_{1s} in Eq. (15), the flow lines, although still having the same planes of constant phase, extend to and return from increasingly larger distances with negligibly small radiant fluxes at the larger distances. It may be of interest in Figs. 4 and 5 to see that the reversibility principle[11] is also valid for inhomogeneous waves, for the reflection and transmission properties at each point of incidence, except for a mirror type image inversion, are

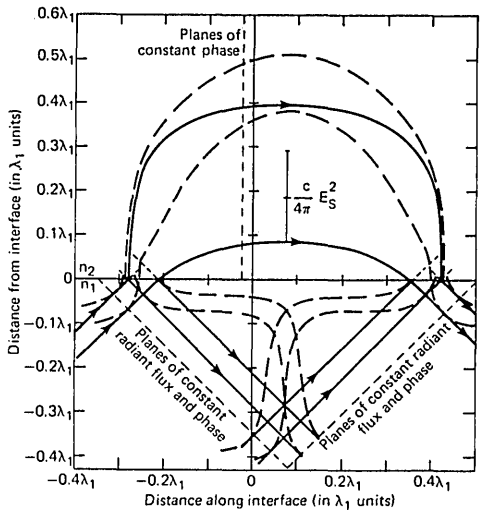

Fig. 5. Radiant flux and radiant flux flow lines for s polarization with $x_{1s} = -0.2087\lambda_1$ and $-0.28\lambda_1$ when $n_1 = 1.5$, $n_2 = 1.0$, $\varphi = 45°$, and $t = 0$.

just the reverse of those at corresponding points of reentrance.

All the previous calculations were carried out with incident $|\mathbf{P}^i(s)|$ radiant fluxes in Eqs. (10) and (16), which were stationary and peaked at $x = z = t = 0$, and these choices fix the origin of the coordinate system in Figs. 2, 3, 4, and 5 along the interface. One must then ask what will happen if the phases of the incident waves in Eqs. (4) are advanced by some arbitrary amount or the time is increased. To answer such a question, clearly one must go back to Eqs. (4), insert some arbitrary phase advance Δ, and repeat all the following calculations. Fortunately, when this is done, Maxwell's equations and the boundary conditions dictate that one must simply insert Δ in all the periodic terms in Eqs. (4) and in all the equations derived from Eqs. (4). If, for example, we advance the phase of the incident wave by $\Delta = 45°$ or $\frac{1}{8}\lambda_1$ and repeat all the calculations in Fig. 2 with this value of Δ inserted in Eqs. (10), Fig. 6 will be obtained. These curves are of precisely the same forms as those in Fig. 2, but each has been moved to the right by the amount

$$\Delta x = \frac{\Delta}{2\pi \sin\varphi}\lambda_1 = 0.1768\lambda_1 \qquad (22)$$

and has new ordinates for the original x values in Fig. 2, which are determined by inserting Δ in Eqs. (10). If all the curves in Fig. 2 are moved to the right by this amount for $\Delta = 45°$, clearly all the other curves in Figs. 3 through 5 must be moved to the right by this same amount. The phases of the waves in Eqs. (4) and (9) can, however, also be advanced by increasing the time. Suppose now we increase the phases of the waves in Eqs. (4) and (9) by increasing the time until $\omega t = 45°$. If we substitute this value for ωt in Eqs. (10) and plot these components of the Poynting vector in a similar way to Fig. 2, we again expect to obtain Fig. 6 with a shift to the right of

$$\Delta x = \frac{\omega t}{2\pi \sin\varphi}\lambda_1 = \frac{V_1}{\sin\varphi}t = 0.1768\lambda_1. \qquad (23)$$

This equation, however, tells us that, for any advance in phase resulting from increases in time, we must move Fig. 6 to the right with a velocity $V_1/\sin\varphi$ for an appropriate time such that $\omega t = 45°$, and the new ordinates in Fig. 6 will be described by Eqs. (10) with either this value of Δx or the corresponding ωt inserted.

The striking things here are the different ways in which the radiant fluxes are predicted to propagate through the two media. To try to show this in more detail, we have in Fig. 7 extended the calculations in Fig. 4 to two adjacent cycles along the interface and have included other appropriate incident and reflected flow lines and radiant fluxes necessary for understanding these processes. Between the outer limiting flow lines in each cyclic group in Eq. (15), we can, as previously suggested, expect infinite numbers of other flow lines

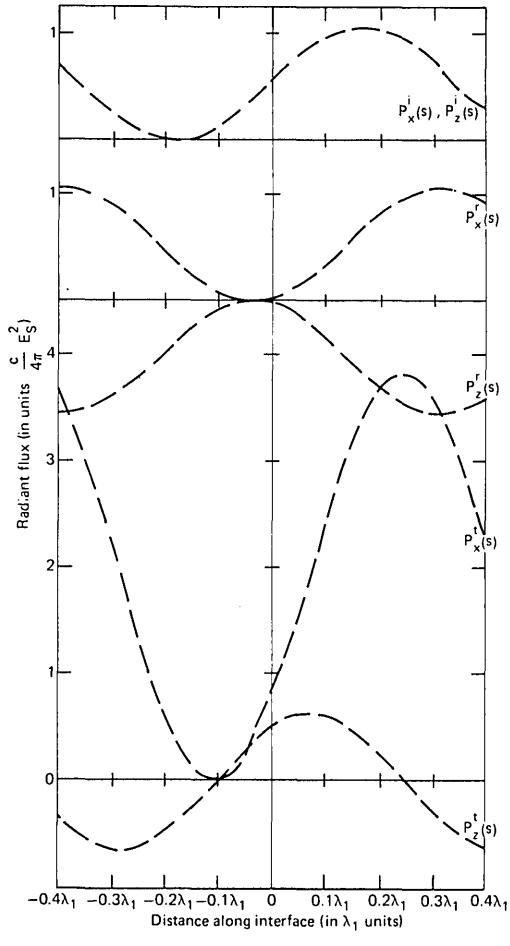

Fig. 6. Components of incident, reflected, and transmitted radiant fluxes for s polarization along interface (in units of λ_1) for $n_1 = 1.5$, $n_2 = 1.0$, $\varphi = 45°$, and $z = t = 0$, but with an advance in phase $\Delta = 45°$.

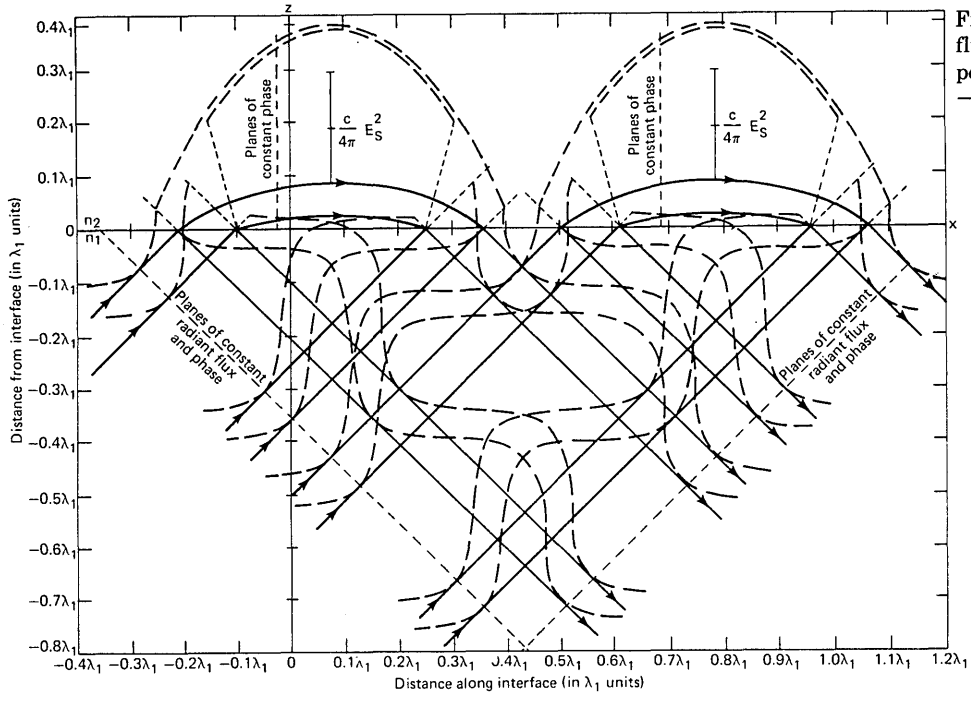

Fig. 7. Radiant flux and radiant flux flow lines for two cycles of s polarization with $x_{1s} = -0.1\lambda_1$ and $-0.2087\lambda_1$ when $n_1 = 1.5$, $n_2 = 1.0$, $\varphi = 45°$, and $t = 0$.

in the second medium of the same shapes and having depths of penetration extending from zero to infinitely large distances. If now, as required by Eqs. (10) and (16), we move Fig. 7 to the right with a velocity $V_1/\sin\varphi$ and, with proper shielding, observe the changes in the incident and reflected radiant fluxes at some fixed (x,z) point in medium one, it should be clear that, during the passage of the first cycle, we will see one complete oscillation in the incident or reflected radiant fluxes in Eqs. (16), as observed along the directions of the flow lines. During the passage of the second cycle, one must again see the same oscillation with no interruption in the magnitudes and phases for the first cycle. These are familiar phenomena associated with unbounded waves propagating through unbounded media. If now an observer with somewhat different shielding and detecting capabilities views the radiant flux propagation at a fixed point in medium two and again Fig. 7 is moved to the right with a velocity $V_1/\sin\varphi$, infinite numbers of curved flow lines, above a lower limiting flow line determined by the z coordinate of the observer, now move across the point of observation at symmetrical positions about their common peak positions. During the passage of the first cycle, one can expect to see one complete oscillation in the radiant flux, whose maximum in Eq. (16) is a function of the z coordinate of the observer, and the second cycle will not add anything new. These are ingenious processes, for incident planes of constant radiant flux and phase in the first medium, after experiencing these complex processes in the second medium, are still able to generate proper planes of constant radiant flux and phase for the reflected radiant fluxes.

Many electromagnetic waves are of very high frequencies, so that, for detection purposes, it becomes necessary to discuss time averages of these radiant fluxes. Fortunately, all these radiant fluxes can be easily integrated and averaged over any arbitrary time interval. If, then, as has been done by others,[2] we integrate and average the radiant fluxes in Eqs. (10) over the time $1/\nu$ in Eqs. (9) for one oscillation in the $\mathbf{E}$ and $\mathbf{H}$ components, we find

$$\overline{|\mathbf{P}^i(s)|} = \frac{c}{4\pi}\frac{n_1}{2}E_s^2,$$

$$\overline{|\mathbf{P}^r(s)|} = \frac{c}{4\pi}\frac{n_1}{2}E_s^2,$$

$$\overline{P_x{}^t(s)} = \frac{c}{4\pi}\frac{2n_1{}^3\sin\varphi\cos^2\varphi}{n_1{}^2 - n_2{}^2}E_s{}^2\exp\left[-\frac{4\pi}{\lambda_1}z\left(\sin^2\varphi - \frac{n_2{}^2}{n_1{}^2}\right)^{1/2}\right],$$

$$\overline{P_z{}^t(s)} = 0.$$

These are the familiar equations used by earlier authors[2] in arriving at their somewhat paradoxial conclusions. These equations are, of course, correct mathematically, but they lose sight of the fact that the $P_z{}^t(s)$ component in Fig. 2 goes through two oscillations and three changes in sign during this $1/\nu$ time interval, indicating varying inflows and outflows of radiant flux across the interface. It is much more informative in Fig. 2 to ask how the time averages in the radiant fluxes in Eqs. (10) change, when $P_z{}^t(s)$ goes from the positive half cycle, corresponding to an averaged inflow of radiant flux, to the adjacent negative half cycle, corresponding to an averaged outflow of radiant flux, for this is more closely associated with these physical processes and provides a more realistic time average. If, then, we integrate and average all the components in Eqs. (10) over the first half cycle for $P_z{}^t(s)$ in Fig. 2, the time interval is $1/4\nu$, and the limits of integration, from Eqs.

(10) and (15), extend from $[(2\pi)/(\omega\lambda_1)]x_{1s}\sin\varphi - [(\delta_s{}^t)/\omega]$ to $[(2\pi)/(\omega\lambda_1)]x_{1s}\sin\varphi - [(\delta_s{}^t)/\omega] + [1/(4\nu)]$. When these integrations and averagings have been done, we find at $z = 0$ that

$$\overline{|\mathbf{P}^i(s)|_{\text{in}}} = \frac{c}{4\pi} n_1 \left(\tfrac{1}{2} + \frac{1}{\pi}\sin 2\delta_s{}^t\right) E_s{}^2,$$

$$\overline{|\mathbf{P}^r(s)|_{\text{in}}} = \frac{c}{4\pi} n_1 \left(\tfrac{1}{2} - \frac{1}{\pi}\sin 2\delta_s{}^t\right) E_s{}^2,$$

$$\overline{P_x{}^t(s)_{\text{in}}} = \frac{c}{4\pi}\frac{2n_1{}^3\sin\varphi\cos^2\varphi}{n_1{}^2 - n_2{}^2} E_s{}^2,$$

$$\overline{P_z{}^t(s)_{\text{in}}} = \frac{c}{4\pi}\frac{4n_1{}^2\cos^2\varphi(n_1{}^2\sin^2\varphi - n_2{}^2)^{1/2}}{\pi(n_1{}^2 - n_2{}^2)} E_s{}^2. \qquad (25)$$

Similar integrating and averaging are also readily done over the adjacent negative cycle in Fig. 2 with limits extending from $[(2\pi)/(\omega\lambda_1)]x_{1s}\sin\varphi - [(\delta_s{}^t)/\omega] + [1/(4\nu)]$ to $[(2\pi)/(\omega\lambda_1)]\ x_{1s}\sin\varphi - [(\delta_s{}^t)/\omega] + [1/(2\nu)]$. The resulting equations are similar in form to Eqs. (25), but the second terms in $|\mathbf{P}^i(s)|_{\text{out}}$ and $|\mathbf{P}^r(s)|_{\text{out}}$ have opposite signs, and $P_z{}^t(s)_{\text{out}}$ is negative. If, then, we average these equations over adjacent in and out cycles or over sufficiently long periods of time, we learn that, in the time average, all the incident radiant flux is reflected and all the radiant flux entering the second medium returns to the first medium. This is a much more informative and realistic conclusion and avoids the earlier controversies.[2]

Electric Vector Parallel to Plane of Incidence

It has already been inferred that total internal reflection for the p polarization will differ from that for the s polarization, and we would like to indicate briefly some of the significant differences. With H_y along the E_y direction in Fig. 1 and $H_x = H_z = 0$, we find that Maxwell's equations in Eqs. (1) reduce to

$$\frac{\partial H_y}{\partial z} = -\frac{\epsilon}{c}\frac{\partial E_x}{\partial t}, \quad \frac{\partial H_y}{\partial x} = \frac{\epsilon}{c}\frac{\partial E_z}{\partial t}, \quad \frac{\partial E_x}{\partial z} - \frac{\partial E_z}{\partial x} = -\frac{1}{c}\frac{\partial H_y}{\partial t}. \qquad (26)$$

These equations can be solved for H_y, and, when this is done, it will be found that H_y must satisfy the same wave equation in Eq. (3), as found for the E_y component for the s polarization. If we write down the solution to the wave equation, when expressed in terms of the parallel E_p component, determine the forms of the other **E** and **H** components for the incident, reflected, and refracted waves in the region beyond the critical angle, and then make the tangential components E_x and H_y continuous across the interface, the real instantaneous incident, reflected, and transmitted **E** and **H** fields are

$$H_y{}^i = n_1 E_p \cos\left[\omega t - \frac{2\pi}{\lambda_1}(x\sin\varphi + z\cos\varphi)\right],$$

$$E_x{}^i = \cos\varphi E_p \cos\left[\omega t - \frac{2\pi}{\lambda_1}(x\sin\varphi + z\cos\varphi)\right],$$

$$E_z{}^i = -\sin\varphi E_p \cos\left[\omega t - \frac{2\pi}{\lambda_1}(x\sin\varphi + z\cos\varphi)\right],$$

$$H_y{}^r = n_1 E_p \cos\left[\omega t - \frac{2\pi}{\lambda_1}(x\sin\varphi - z\cos\varphi) + \delta_p{}^r\right], \qquad (27)$$

$$E_x{}^r = -\cos\varphi E_p \cos\left[\omega t - \frac{2\pi}{\lambda_1}(x\sin\varphi - z\cos\varphi) + \delta_p{}^r\right],$$

$$E_z{}^r = -\sin\varphi E_p \cos\left[\omega t - \frac{2\pi}{\lambda_1}(x\sin\varphi - z\cos\varphi) + \delta_p{}^r\right],$$

$$H_y{}^t = \frac{2n_1 n_2{}^2\cos\varphi}{(n_1{}^2 - n_2{}^2)^{1/2}[(n_1{}^2 + n_2{}^2)\sin^2\varphi - n_2{}^2]^{1/2}} E_p \times \exp\left[-\frac{2\pi}{\lambda_1} z\left(\sin^2\varphi - \frac{n_2{}^2}{n_1{}^2}\right)^{1/2}\right] \cos\left(\omega t - \frac{2\pi}{\lambda_1} x\sin\varphi + \delta_p{}^t\right),$$

$$E_x{}^t = \frac{2n_1\cos\varphi(n_1{}^2\sin^2\varphi - n_2{}^2)^{1/2}}{(n_1{}^2 - n_2{}^2)^{1/2}[(n_1{}^2 + n_2{}^2)\sin^2\varphi - n_2{}^2]^{1/2}} E_p \times \exp\left[-\frac{2\pi}{\lambda_1} z\left(\sin^2\varphi - \frac{n_2{}^2}{n_1{}^2}\right)^{1/2}\right] \sin\left(\omega t - \frac{2\pi}{\lambda_1} x\sin\varphi + \delta_p{}^t\right),$$

$$E_z{}^t = \frac{2n_1{}^2\sin\varphi\cos\varphi}{(n_1{}^2 - n_2{}^2)^{1/2}[(n_1{}^2 + n_2{}^2)\sin^2\varphi - n_2{}^2]^{1/2}} E_p \times \exp\left[-\frac{2\pi}{\lambda_1} z(\sin^2\varphi - \frac{n_2{}^2}{n_1{}^2})^{1/2}\right] \cos\left(\omega t - \frac{2\pi}{\lambda_1} x\sin\varphi + \delta_p{}^t\right),$$

where the phase changes after reflection and transmission are

$$\tan\frac{\delta_p{}^r}{2} = \tan\delta_p{}^t = \frac{n_1(n_1{}^2\sin^2\varphi - n_2{}^2)^{1/2}}{n_2{}^2\cos\varphi}. \qquad (28)$$

The waves in the second medium are again inhomogeneous waves, with planes of constant phase normal to the x, planes of constant amplitude normal to z, but now have a longitudinal $E_x{}^t$ component.

From these equations, we can also write down the real instantaneous components of the Poynting vector, and it is clear again that we are only going to have P_x and P_z components, which are

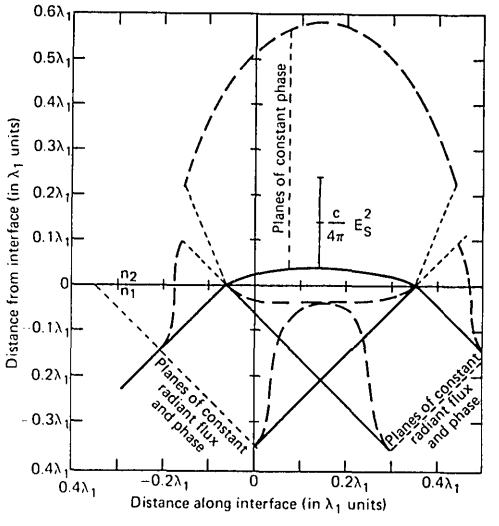

Fig. 8. Radiant flux and radiant flux flow line for p polarization with $x_{1p} = -0.0639\lambda_1$, when $n_1 = 1.5$, $n_2 = 1.0$, $\varphi = 45°$, and $t = 0$.

$$P_x{}^i(p) = \frac{c}{4\pi} n_1 \sin\varphi E_p{}^2 \cos^2\left[\omega t - \frac{2\pi}{\lambda_1}(x\sin\varphi + z\cos\varphi)\right],$$

$$P_z{}^i(p) = \frac{c}{4\pi} n_1 \cos\varphi E_p{}^2 \cos^2\left[\omega t - \frac{2\pi}{\lambda_1}(x\sin\varphi + z\cos\varphi)\right],$$

$$P_x{}^r(p) = \frac{c}{4\pi} n_1 \sin\varphi E_p{}^2 \cos^2\left[\omega t - \frac{2\pi}{\lambda_1}(x\sin\varphi - z\cos\varphi) + \delta_p{}^r\right],$$

$$P_z{}^r(p) = -\frac{c}{4\pi} n_1 \cos\varphi E_p{}^2 \cos^2\left[\omega t - \frac{2\pi}{\lambda_1}(x\sin\varphi - z\cos\varphi) + \delta_p{}^r\right],$$

$$P_x{}^t(p) = \frac{c}{4\pi}\frac{4n_1{}^3 n_2{}^2 \sin\varphi\cos^2\varphi}{(n_1{}^2 - n_2{}^2)[(n_1{}^2 + n_2{}^2)\sin^2\varphi - n_2{}^2]} E_p{}^2 \times \exp\left[-\frac{4\pi}{\lambda_1} z\left(\sin^2\varphi - \frac{n_2{}^2}{n_1{}^2}\right)^{1/2}\right]\cos^2\left[\omega t - \frac{2\pi}{\lambda_1} x\sin\varphi + \delta_p{}^t\right),$$

$$P_z{}^t(p) = \frac{c}{4\pi}\frac{4n_1{}^2 n_2{}^2 \cos^2\varphi (n_1{}^2\sin^2\varphi - n_2{}^2)^{1/2}}{(n_1{}^2 - n_2{}^2)[(n_1{}^2 + n_2{}^2)\sin^2\varphi - n_2{}^2]} E_p{}^2 \times \exp\left[-\frac{4\pi}{\lambda_1} z\left(\sin^2\varphi - \frac{n_2{}^2}{n_1{}^2}\right)^{1/2}\right] \times \sin\left(\omega t - \frac{2\pi}{\lambda_1} x\sin\varphi + \delta_p{}^t\right)\cos\left(\omega t - \frac{2\pi}{\lambda_1} x\sin\varphi + \delta_p{}^t\right). \quad (29)$$

The $\mathbf{P}^i(p)$ components, except for a different incident amplitude E_p, are of the same forms as the $\mathbf{P}^i(s)$ components in Eqs. (10). The $\mathbf{P}^r(p)$ components are also similar in form to the $\mathbf{P}^r(s)$ components, but the phase changes after reflection are different, so that the $\mathbf{P}^r(p)$ components will be shifted to the right in Fig. 2 by

$$\Delta x = \frac{\lambda_1}{2\pi\sin\varphi}(\delta_p{}^r - \delta_s{}^r) \quad (30)$$

from the corresponding $\mathbf{P}^r(s)$ components. For the $\mathbf{P}^t(p)$ components, one must also expect a shift to the right of

$$\Delta x = \frac{\lambda_1}{2\pi\sin\varphi}(\delta_p{}^t - \delta_s{}^t), \quad (31)$$

but the ordinates of the $\mathbf{P}^t(p)$ components are larger than the $\mathbf{P}^t(s)$ components in Fig. 2 due to the factor $n_2{}^2/[(n_1{}^2 + n_2{}^2)\sin^2\varphi - n_2{}^2]$. The slopes and forms of the p flow lines can be determined, using the same methods as for the s polarization. These considerations show that the incident and reflected flow lines are of the same form as for the s polarization in Eqs. (11) and (12). In the second medium, however, we see from Eqs. (29)

$$\left(\frac{dz}{dx}\right)_t = \frac{P_z{}^t(p)}{P_x{}^t(p)} = \frac{(n_1{}^2\sin^2\varphi - n_2{}^2)^{1/2}}{n_1\sin\varphi}\tan\left(\omega t - \frac{2\pi}{\lambda_1} x\sin\varphi + \delta_p{}^t\right),$$

$$z^t(p) = \frac{\lambda_1(n_1{}^2 sin^2\varphi - n_2{}^2)^{1/2}}{2\pi n_1 sin^2\varphi}\left\{log_e\left[\cos\left(\omega t - \frac{2\pi}{\lambda_1} x\sin\varphi + \delta_p{}^t\right)\right] - \log_e\left[\cos\left(\omega t - \frac{2\pi}{\lambda_1} x_{1p}\sin\varphi + \delta_p{}^t\right)\right]\right\}. \quad (32)$$

The flow lines for the p polarization in the second medium will then for the same x_{1s} and x_{1p}, have the same shapes as those for the s polarization, but they will be shifted to the right by the amount indicated in Eq. (31) and have different penetration depths.

To give a brief indication of other differences between the two polarizations, we have in Fig. 8 plotted calculated instantaneous $|\mathbf{P}^i(p)|$, $|\mathbf{P}^r(p)|$, and $|\mathbf{P}^t(p)|$ radiant fluxes along their appropriate flow lines, as obtained from Eqs. (29) and (32), for which there were no reflection losses along the interface. This choice was made so that a comparison could be made with the corresponding s polarization in Fig. 4. From Eqs. (17), (18), and (19), we find for a p flow line with these properties that $x_{1p} = -0.0639\lambda_1, x_{2p} = 0.3536\lambda_1$ and the peak radiant flux appears at $x = 0.1448\lambda_1$, as shown in Fig. 8. This flow line, although exhibiting no reflection losses along the interface, has properties quite different from the corresponding s flow line, for it has a discontinuity in the radiant flux at the interface, is refracted in crossing the interface, has a different penetration depth, is shifted to the right by the amount indicated in Eq. (31) and has a much larger radiant flux flow, due to the previously mentioned multiplication factor. The discontinuity in the radiant fluxes is of the familiar form for which the normal components are continuous and the tangential components discontinuous, as is necessary in order to have refraction. This one sampling of the radiant fluxes and flow lines indicates that we can expect the p flow lines to have the same shapes and different penetration depths, but they will all be displaced to the right by the amount suggested in Eq. (31), and the radiant fluxes along these flow lines and the boundary conditions at the points of incidence and reentrance into the first medium will all be expected to differ from the s polarization. It is, of course, proper, from the viewpoint of physical optics, for the p polarization to be moved to the right by this amount, for elliptically polarized radiant fluxes must appear, when Fig. 7, with both polarizations present, is moved to the right with a velocity $V_1/\sin\varphi$.

One other problem with somewhat broader implications remains. If we have a plane surface which is black over a solid angle π and responds only to long time averages in the radiant flux, it is of interest to know what such a surface might see in the second medium for the two polarizations, when it is moved up close, but not in contact at the interface, and how such a surface might be expected to modify the reflected radiant flux in the first medium. With regard to the first problem, it should be clear from Eqs. (10) and (25) that, if we integrate and average over adjacent in and out cycles for a fixed z, the time averages of the radiant fluxes for the s components seen in the second medium will be

$$\overline{P_x{}^t(s)} = \frac{c}{4\pi}\frac{2n_1{}^3\sin\varphi\cos^2\varphi}{n_1{}^2 - n_2{}^2} E_s{}^2 \exp\left[-\frac{4\pi}{\lambda_1} z\left(\sin^2\varphi - \frac{n_2{}^2}{n_1{}^2}\right)^{1/2}\right],$$

$$\overline{P_z{}^t(s)} = \frac{c}{4\pi}\frac{2n_1{}^2\cos\varphi(n_1{}^2\sin^2\varphi - n_2{}^2)^{1/2}}{\pi(n_1{}^2 - n_2{}^2)} E_s{}^2 \times \exp\left[-\frac{4\pi}{\lambda_1} z\left(\sin^2\varphi - \frac{n_2{}^2}{n_1{}^2}\right)^{1/2}\right]. \quad (33)$$

The specific assumption made here is that the surface sees no radiant flux moving toward the interface in the out cycle in Eqs. (25), so that the above $\overline{P_z{}^t(s)}$ is simply one half of the predicted $\overline{P_z{}^t(s)}_{\text{in}}$ at the z value in question. Similar integrating and averaging for the p components in Eqs. (29) will yield $\overline{P_x{}^t(p)}$ and $\overline{P_z{}^t(p)}$ components of the same form, but with the previously indicated multiplication factor. In Fig. 9, we have given

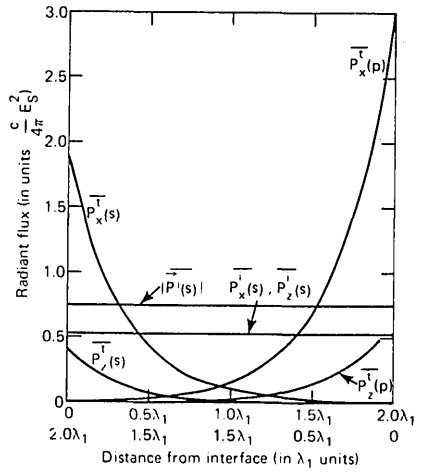

Fig. 9. Time averages of s and p radiant fluxes in second medium at different distances from interface with $E_p = E_s$, $n_1 = 1.5$, $n_2 = 1.0$, and $\varphi = 45°$.

some calculated $\overline{P_x{}^t(s)}$, $\overline{P_z{}^t(s)}$, $\overline{P_x{}^t(p)}$, and $\overline{P_z{}^t(p)}$ values for varying z positions, when $E_p = E_s$. The abscissae for the two polarizations are in units of λ_1, but those for the s polarization must be viewed from left to right, while those for the p polarization must be viewed from right to left. It is clear from these calculations that $\overline{P_x{}^t(s)}$ and $\overline{P_x{}^t(p)}$ are much larger than the $\overline{P_z{}^t(s)}$ and $\overline{P_z{}^t(p)}$, so that the radiant flux flow in the time average is predominantly along a direction parallel to the boundary in the second medium. We see also that $\overline{P_x{}^t(s)}$ and $\overline{P_x{}^t(p)}$ are much larger than $|\overline{\mathbf{P}^i(s)}|$, indicated in the lower part of the figure, so that the refraction properties and flow line shapes in the second medium increase the flow line densities along the x direction, when compared with the corresponding flow line density along the incident radiant flux. We find also that $\overline{P_x{}^t(p)} > \overline{P_x{}^t(s)}$ and $\overline{P_z{}^t(p)} > \overline{P_z{}^t(s)}$, so that the radiant flux for the p polarization is more successful in passing through the interface, as is also the case for more familiar problems.[12]

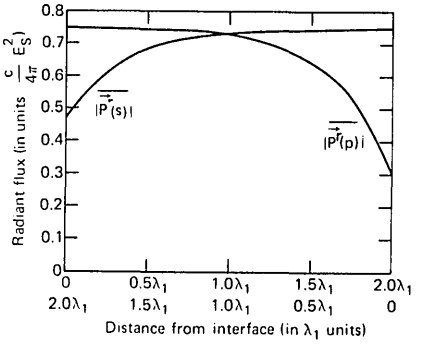

Fig. 10. Time averages of s and p reflected radiant fluxes in first medium, when a perfectly black absorbing surface is moved from $z = 2.0\lambda_1$, to $z = 0$ with $E_p = E_s$, $n_1 = 1.5$, $n_2 = 1.0$, and $\varphi = 45°$.

To determine just how such an absorbing surface might be expected to affect the reflected radiant fluxes, we must, for the s polarization, return to Eqs. (13), (14), and (25). For the in cycle, it is clear that the radiant flux flow across the interface is not going to be affected by the absorbing surface, so that Eqs. (25) in their present forms will also be useful here. For the out cycle, however, $\overline{P_z{}^i(s)}_{\text{out}}$ must still be the same, but $\overline{P_z{}^t(s)}_{\text{out}}$ and $\overline{P_z{}^r(s)}_{\text{out}}$ will be different. We have already seen in Eqs. (33) that the role of the absorbing surface is simply that of absorbing all the radiant flux incident upon it. For the remaining unperturbed flow lines returning to the interface, the out cycle must then be

$$\overline{|\mathbf{P}^i(s)|}_{\text{out}} = \frac{c}{4\pi} n_1 \left(\tfrac{1}{2} - \frac{1}{\pi}\sin 2\delta_s{}^t\right) E_s{}^2,$$

$$\overline{|\mathbf{P}^r(s)|}'_{\text{out}} = \frac{c}{4\pi} n_1 \left(\tfrac{1}{2} + \frac{1}{\pi}\sin 2\delta_s{}^t\right)(1 - f_s) E_s{}^2,$$

$$\overline{P_x{}^t(s)}'_{\text{out}} = \frac{c}{4\pi}\frac{2n_1{}^3 \sin\varphi \cos^2\varphi}{n_1{}^2 - n_2{}^2} E_s{}^2 \times \left\{1 - \exp\left[-\frac{4\pi}{\lambda_1} z \left(\sin^2\varphi - \frac{n_2{}^2}{n_1{}^2}\right)^{1/2}\right]\right\},$$

$$\overline{P_z{}^t(s)}' = -\frac{c}{4\pi}\frac{4n_1{}^2 \cos^2\varphi (n_1{}^2 \sin^2\varphi - n_2{}^2)^{1/2}}{\pi(n_1{}^2 - n_2{}^2)} \times E_s{}^2 \left\{1 - \exp\left[-\frac{4\pi}{\lambda_1} z \left(\sin^2\varphi - \frac{n_2{}^2}{n_1{}^2}\right)^{1/2}\right]\right\}, \quad (34)$$

where f_s is a factor determined by the boundary conditions. If in Eq. (14) we make the time averages of the normal components of the radiant flux continuous across the boundary, f_s becomes

$$f_s = \frac{4n_1 \cos\varphi (n_1{}^2 \sin^2\varphi - n_2{}^2)^{1/2}}{\pi(n_1{}^2 - n_2{}^2)\left(\tfrac{1}{2} + \frac{1}{\pi}\sin 2\delta_s{}^t\right)} \times \exp\left[-\frac{4\pi}{\lambda_1} z \left(\sin^2\varphi - \frac{n_2{}^2}{n_1{}^2}\right)^{1/2}\right]. \quad (35)$$

To obtain the time average of the radiant fluxes in this particular case, we must average the in and out cycles in Eqs. (25) and (34), so that

$$|\mathbf{P}^i(s)| = \frac{c}{4\pi}\frac{n_1}{2} E_s{}^2,$$

$$|\mathbf{P}^r(s)| = \frac{c}{4\pi}\frac{n_1}{2}\left[1 - \left(\tfrac{1}{2} + \frac{1}{\pi}\sin 2\delta_s{}^t\right) f_s\right] E_s{}^2,$$

$$P_x{}^t(s) = \frac{c}{4\pi}\frac{2n_1{}^3 \sin\varphi \cos\varphi}{n_1{}^2 - n_2{}^2} \times \left\{1 - \tfrac{1}{2}\exp\left[-\frac{4\pi}{\lambda_1} z \left(\sin^2\varphi - \frac{n_2{}^2}{n_1{}^2}\right)^{1/2}\right]\right\} E_s{}^2,$$

$$P_z{}^t(s) = \frac{c}{4\pi}\frac{2n_1{}^2 \cos^2\varphi (n_1{}^2 \sin^2\varphi - n_2{}^2)^{1/2}}{\pi(n_1{}^2 - n_2{}^2)} E_s{}^2 \times \exp\left[-\frac{4\pi}{\lambda_1} z \left(\sin^2\varphi - \frac{n_2{}^2}{n_1{}^2}\right)^{1/2}\right]\Bigg\}. \quad (36)$$

These equations describe the time averages of the radiant flux flow in both media for varying z distances of the absorbing surface from the interface. Similar equations for the p polarization can also be obtained by replacing E_s by E_p, $\delta_s{}^t$ by $\delta_p{}^t$, f_s by f_p and inserting the multiplication factor in $\overline{P_x{}^t(s)}$ and $\overline{P_z{}^t(s)}$. The new

factor f_p is obtained from f_s by also replacing $\delta_s{}^t$ by $\delta_p{}^t$ and inserting the before mentioned multiplication factor. These are interesting equations, but we are only committed to discuss how $|\overline{\mathbf{P}^r(s)}|$ and $|\overline{\mathbf{P}^r(p)}|$ change as the absorbing surface is brought up to the interface without making optical contact. We have, therefore, in Fig. 10 plotted some calculated $|\overline{\mathbf{P}^r(s)}|$ and $|\overline{\mathbf{P}^r(p)}|$ values for different z distances of the absorbing surface from the interface. At large distances, Eqs. (36) go over into Eqs. (24), so that the $|\overline{\mathbf{P}^r(s)}|$ values approach the upper limit $[c/(8\pi)]n_1E_s{}^2$ at which the absorbing surface has no effect on the reflected radiant flux. As the absorbing surface is moved closer to the interface, the increasing exponential terms in f_s introduce losses in $|\overline{\mathbf{P}^r(s)}|$ which increase as z decreases. At $z = 0$, where the $|\overline{\mathbf{P}^t(s)}|_{\text{out}}$ components vanish in Eqs. (34), the reflected $|\overline{\mathbf{P}^r(s)}|$ components in Eqs. (36) have two contributing components, $|\overline{\mathbf{P}^r(s)}|_{\text{in}}$ and $|\overline{\mathbf{P}^i(s)}|$, in Eqs. (36) and reach their minimum value at this point. The $|\overline{\mathbf{P}^r(p)}|$ in Fig. 10 yield similar results, but the losses at smaller z values are greater, due to the presence of the p polarization multiplication factor in f_p, if we set $E_p = E_s$. There are other interesting phenomena to be explored here.

Conclusions

In this paper, we have supplied a much needed solution for total internal reflection, which gives a clear picture of the physical processes involved. This was done by using boundary value problem techniques, of the same form used in deriving Fresnel's equations,[13] and by looking at the flow lines and associated radiant fluxes at different points along the interface in the stationary, time changing, and time averaged states. Our theory shows in the stationary sense that all the radiant flux is not reflected at the interface, but that both reflection and transmission simultaneously appear. The transmitted radiant fluxes, however, follow curved paths in the second medium and reenter the first medium in such a way that the incident radiant fluxes, in conjunction with the specularly reflected radiant fluxes, give the appearance of being completely reflected at the interface. For both polarizations, the flow lines in the two media have the same forms, but those for the p polarization are advanced along the interface by an amount depending upon their differences in phase in crossing the interface. The radiant fluxes along these flow lines and the boundary conditions for the two polarizations at the points of incidence and reentrance, however, are quite different. All these unusual reflection, refraction, and propagation characteristics are due to the inhomogeneous waves in the second medium, and it was interesting to the authors to see how incident planes of constant radiant flux and phase experienced such complex processes in the second medium and were still capable of generating reflected planes of constant radiant flux and phase in the first medium. To show how the radiant fluxes change with time in both media, the theory indicates that the periodic arrays of stationary flow lines and radiant fluxes must be moved along the interface with a velocity $V_1/\sin\varphi$, and the magnitudes and phases of these radiant fluxes observed at fixed points in either medium. For cases in which the time constant of the detecting device is long compared with time for one oscillation in the radiant flux, we have also calculated the time averages of the radiant fluxes in both media and have determined how an absorbing plate, when placed close to the interface in air, might affect the reflected radiant fluxes. By proceeding in this way, we have been able to provide a much more informative and realistic description of the physical processes involved in total internal reflection and remove many of the earlier difficulties. There will, of course, be other questions, but we hope that these ideas will provide a deeper insight into these problems and aid in their solution.

This paper was presented at the annual meeting of the Optical Society of America, in Toronto, October 1977.

The authors are indebted to W. G. Fastie of the Johns Hopkins University, who originally suggested this problem. A discussion with R. W. Hart of the Applied Physics Laboratory on some closely related material resulted in a similar suggestion. The authors are indebted to D. L. George also of the Applied Physics Laboratory for the art work and to L. Holtschlag for help with the Russian translation.

This work was supported in part by the Department of the Navy, Naval Sea Systems Command under contract N00017-72-4401.

References

1. H. K. V. Lotsch, J. Opt. Soc. Am. **58**, 551 (1968); Optik **32**, 116, 189 (1970); **32**, 299, 553 (1971).
2. H. Geiger and K. Scheel, *Handbuch der Physik* (Julius Springer, Berlin, 1928), Vol. 20, p. 228; C. Schaefer, *Einfuhrung die theoretische Physik* (W. de Gruyter, Berlin, 1949), Vol. 3, p. 406; M. Born and E. Wolf, *Principles of Optics* (Pergamon, New York, 1959), p. 47.
3. M. Born and E. Wolf, *Principles of Optics* (Pergamon, New York, 1959), p. 112.
4. W. Culshaw and D. S. Jones, Proc. Phys. Soc. London, Sect. B **66**, 859 (1954); H. Osterberg and L. W. Smith, J. Opt. Soc. Am. 1073 (1964).
5. C. Schaefer and G. Gross, Ann. Phys. **32**, 648 (1910).
6. J. A. Stratton, *Electromagnetic Theory* (McGraw-Hill, New York, 1941), p. 34.
7. M. Born, *Optik* (Julius Springer, Berlin, 1933), p. 41.
8. H. Geiger and K. Scheel, *Handbuch der Physik* (Springer, Berlin, 1928), Vol. 20, p. 194.
9. A. Eichenwald, J. Russ. Phys. Chem. **4**, 137 (1919).
10. M. Born, Optik (Julius Springer, Berlin, 1933), p. 31.
11. G. G. Stokes, Cambridge Math. J. **8**, 1 (1849).
12. F. A. Jenkins and H. E. White, *Fundamentals of Physical Optics* (McGraw-Hill, New York, 1937), p. 390.
13. M. Born, *Optik* (Springer, Berlin, 1933), p. 29.